Computer Physics Communications 137 (2001) 286–299

Computer Physics Communications

www.elsevier.nl/locate/cpc

An improved masking method for absorbing boundaries in electromagnetic particle simulations

Takayuki Umeda, Yoshiharu Omura *, Hiroshi Matsumoto

Radio Science Center for Space and Atmosphere, Kyoto University, Uji, Kyoto 611-0011, Japan

Received 11 December 2000; received in revised form 24 January 2001; accepted 26 January 2001

Abstract

We have developed a new scheme to mask electromagnetic fields for absorbing boundaries used in electromagnetic particle codes. The conventional masking method can suppress reflection of various plasma waves by assigning large damping regions for absorbing boundaries. It requires substantial computer memory and processing time. We introduce two new parameters to control absorption of outgoing electromagnetic waves. The first parameter is a damping parameter to change the effective length of damping regions. The second parameter is a retarding parameter to change phase velocities of electromagnetic waves in the damping regions. As a new masking method, we apply both damping and retarding factors. We also found that the best absorption of outgoing waves is realized with a combination of a smaller damping factor and a larger retarding factor. The new method allows us to reduce the size of damping regions substantially.

PACS: 02.70; 52.65.R

Keywords: Absorbing boundary conditions; EM PIC code

1. Introduction

In particle simulations of space plasmas, both periodic and open systems are used for studies of nonlinear wave-particle interaction in space plasmas. Periodic systems are used to simulate micro-scale phenomena such as time evolution of infinite uniform systems. On the other hand, large-scale phenomena such as spatial evolution of localized perturbation are studied in open systems rather than periodic systems. Open systems are regarded as one part of an infinite space. Boundary conditions of open systems are called ‘open’ or ‘free’ boundaries. Since we pick up a segment of real space plasmas as a ‘simulation box’, we need a special numerical treatment of the boundaries between the simulation box and the surrounding outer region. A requirement for open boundary conditions is to behave as if there were no boundaries. An important problem in simulation studies in open systems is reflection of electromagnetic waves at boundaries. There have been a number of studies on boundary conditions which can suppress reflection of outgoing waves (e.g., [1,2]). They are called ‘absorbing boundaries’.

* Corresponding author.

E-mail addresses: umeda@kurasc.kyoto-u.ac.jp (T. Umeda), omura@kurasc.kyoto-u.ac.jp (Y. Omura), matsumot@kurasc.kyoto-u.ac.jp (H. Matsumoto).

0010-4655/01/$ – see front matter
PII: S0010-4655(01)00182-5

Algorithms of absorbing boundaries fall into two categories. In the algorithms in the first category (e.g., [3, 4]), boundaries are simulated by assuming that outgoing electromagnetic waves have a certain phase velocity. Scalar wave equations are solved to approximate boundary values so that outgoing waves are not reflected at the boundaries. While there are many kinds of plasma waves which have different frequencies and phase velocities, the algorithms in the first category can only absorb a single wave mode.

The algorithms in the second category are to absorb outgoing waves using a resistive medium such as a dielectric. In laboratory experiments, so called a wave absorber is located on the wall. In particle simulations, the 'masking method' (damping region method) [5] is used. In this method, outgoing waves are artificially damped by simple masking of electromagnetic fields in 'damping regions' attached at both ends of the simulation box. While the masking method is a useful scheme which can suppress reflection of various plasma waves at boundaries, this method has the following weak point. Electromagnetic waves that propagate through a resistive layer can be completely absorbed if the thickness of the layer is large enough. A larger resistive layer gives better absorption. Therefore, the absorbing boundaries in the second category requires substantial computer memory and processing time.

In the present study, we avoid the weak point of the masking method by developing an improved scheme of the masking method. In Section 2, we first investigate the characteristics of the conventional masking method. We introduce a new masking parameter to control effective length of damping regions. The characteristics of the improved masking method with the effective damping regions are also investigated in this section. In Section 3, we introduce one more parameter and use two different masking factors to absorb outgoing waves. We also try to obtain the most effective combination of the two masking factors. Section 4 gives summary and conclusion.

2. Effective damping region

In the present study, we used Kyoto university one-dimensional ElectroMagnetic Particle cOde (KEMPO1) [6]. The masking method is adopted in KEMPO for about two decades because it is easily implement in the simulation code. The simulation model is schematically illustrated in Fig. 1. The simulation system is taken along the x-axis. The system consists of a physical region and damping regions. The damping regions are attached at both ends of the physical region. The external (static) magnetic field B_0 is taken in the x–y plane. The amplitude of B_0 is given by

$$\left.\begin{aligned} B_{0x} &= \frac{\Omega_e}{(q/m_e)}\cos\theta \\ B_{0y} &= \frac{\Omega_e}{(q/m_e)}\sin\theta \end{aligned}\right\} \tag{1}$$

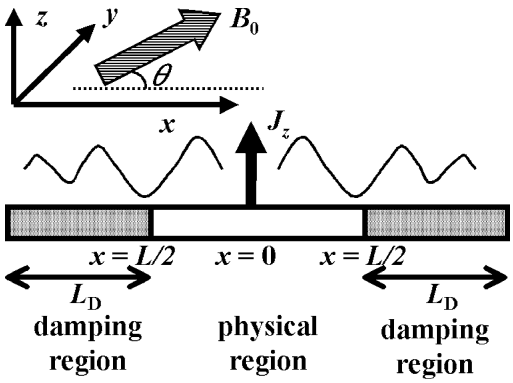

Fig. 1. Simulation model. Electromagnetic waves are radiated at the center of the simulation system and absorbed in the damping regions.

where Ω_e, q/m_e and θ are electron cyclotron frequency, electron charge-to-mass ratio and the angle between B_0 and the x-axis, respectively. We assume a current source at the center of the simulation system. The external current J_0 is driven in the z-direction and electromagnetic waves are radiated in the system. The current J_0 is given by

$$J_0 = \begin{cases} A_J \sin(\omega_J t) & \text{for } 0 \leqslant t \leqslant 2\pi/\omega_J, \\ 0 & \text{for } t > 2\pi/\omega_J, \end{cases} \tag{2}$$

where A_J and ω_J are the amplitude and frequency, respectively. As the initial condition, all electrons in the system form a Maxwellian velocity distribution given by

$$f(v) = \frac{N}{\sqrt{2\pi}V_{th}} \exp\left(-\frac{v^2}{2V_{th}^2}\right), \tag{3}$$

where N and V_{th} are density and thermal velocity, respectively. Ions are assumed to be uniform neutralizing background with an infinite mass in the simulation system. The common parameters for all simulation runs are listed below.

Grid spacing	$\Delta x \cdot \omega_J/c = 0.02$;
Time step	$\omega_J \Delta t = 0.016$;
Length of physical region	$L \cdot \omega_J/c = 20.48$;
Debye length	$\lambda_D \cdot \omega_J/c = 0.02$;

where $\lambda_D = V_{th}/\Pi_e$. These values are normalized by the frequency of the driving current ω_J and the light speed c. We use 1024 superparticles for one grid point.

We generate three type of plasma waves varying electron plasma frequency Π_e, electron cyclotron frequency Ω_e and θ. The parameters for the three modes are listed in Table 1. Run (a) corresponds to light mode, i.e. electromagnetic waves in vacuum. Whistler mode and X-mode waves are excited is runs (b) and (c), respectively, as indicated by their dispersion relations shown in Fig. 2.

Outgoing waves are absorbed by simple masking electromagnetic fields in the damping regions. In other words, their amplitude are gradually reduced by multiplying a masking function f_M to the right-hand side of the time difference form of Maxwell's equations at each time step, written as,

$$\left.\begin{aligned} \boldsymbol{B}^{t+\Delta t/2}(x) &= \left\{\boldsymbol{B}^{t-\Delta t/2}(x) - \Delta t(\nabla \times \boldsymbol{E}^t(x))\right\} \cdot f_M(x) \\ \boldsymbol{E}^{t+\Delta t/2}(x) &= \left\{\boldsymbol{E}^{t-\Delta t/2}(x) - \Delta t(\boldsymbol{J}^t(x) - c^2\nabla \times \boldsymbol{B}^t(x))\right\} \cdot f_M(x) \end{aligned}\right\} \tag{4}$$

Table 1
Simulation parameters varied for different runs

Run	Π_e/ω_J	Ω_e/ω_J	θ
(a)	0.0	0.0	0°
(b)	10.0	10.0	0°
(c)	2.0	8.0	90°

ω_J is the frequency of the driving current.

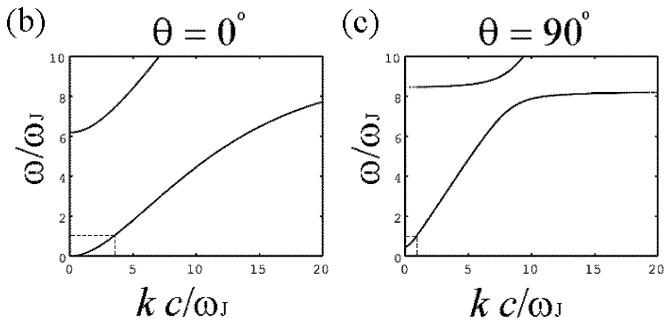

Fig. 2. Dispersion relation of run (b) (left) and run (c) (right) in Table 1. The dashed lines show the parameter of simulation runs. Whistler mode and X-mode waves are generated from the parameter run (b) and (c), respectively.

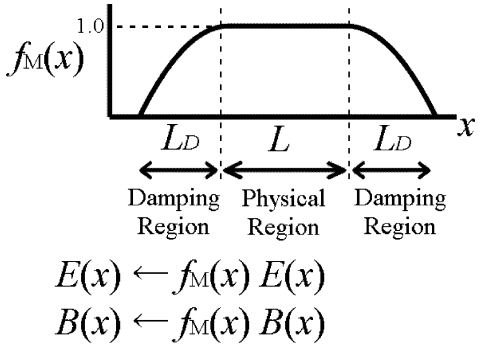

Fig. 3. Masking function and procedure of the masking method. L and L_{D} represent lengths of the physical and damping regions, respectively.

We use a parabolic masking function with $f_{\mathrm{M}} = 1$ in physical region and $f_{\mathrm{M}} < 1$ in damping regions. f_{M} vary gradually from 1 to smaller value closer to the boundary. The masking function and procedure of the masking method are schematically illustrated in Fig. 3. The masking function is given by

$$f_{\mathrm{M}}(x,r) = \begin{cases} 1 & \text{for } |x| \leqslant \frac{L}{2}, \\ 1 - \left(r\frac{|x|-L/2}{L_{\mathrm{D}}}\right)^2 & \text{for } |x| > \frac{L}{2}, \end{cases} \tag{5}$$

where L_{D} $(= N_{\mathrm{D}}\Delta x)$ represents length of damping regions. We introduce a new masking parameter r $(0 < r \leqslant 1)$ to change the gradient of the function. The masking function f_{M} becomes 0 at $x = \pm(L/2 + L_{\mathrm{D}}/r)$. As shown in Fig. 4, L_{D}/r represents length of the 'effective' damping region. We define the masking parameter r by

$$r = \frac{\text{Length of real damping region}}{\text{Length of effective damping region}}. \tag{6}$$

In the conventional masking method, the masking function (5) is used with $r = 1.0$.

Firstly, we use the conventional method and change the length of the damping regions L_{D} to study the reflection ratio of light mode, whistler mode and X-mode waves. As one of simulation results, we show the spatial and time profile of intensity of the three plasma waves for $L_{\mathrm{D}} = 320$ in Fig. 5. We compute magnetic field energy $|B_y^2 + B_z^2|$ at each grid point and time step. Space is normalized by the wavelength of light mode waves $\lambda = 2\pi c/\omega$. In the present study, $\lambda = 314$. Time is normalized by the frequency of external current ω_J. The intensity of magnetic field is normalized by amplitude of incident waves. The size of damping region is indicated by the thick lines above the

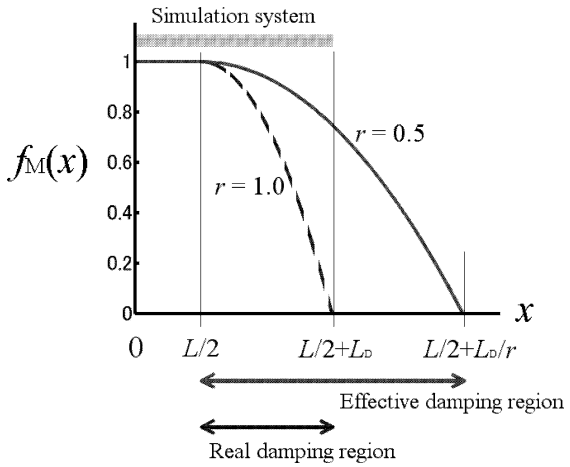

Fig. 4. Shape of the masking function (5) for different r. The dashed and solid lines correspond to $r = 1.0$ and $r = 0.5$, respectively. Length of the effective damping region is given by L_D/r.

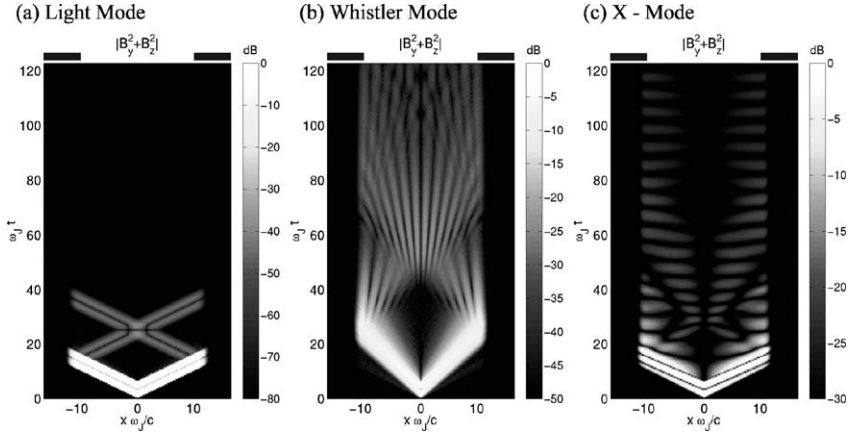

Fig. 5. Spatial and time profiles of magnetic field energy, $|B^2|$, of light mode (left), whistler mode (center), X-mode waves (right), respectively. The masking function (5) with $r = 1.0$ is applied to 320 grid points in each damping region. The sizes of the damping region are shown by the lines above the figures.

figures. As shown in Fig. 5, electromagnetic waves are radiated at the center of the system and propagate to the boundary. While they are absorbed in the damping regions, some waves are reflected in the damping regions.

To calculate the reflection ratio, we specify two regions in the space-time plane for incident and reflected waves, respectively, as schematically illustrated in Fig. 6. The reflection ratio Γ is given by the integration of magnetic field energy in the specified regions, as follows:

$$\Gamma = 10 \times \log_{10} \frac{I_{\text{reflect}}}{I_{\text{in}}} \quad [\text{dB}], \tag{7}$$

$$I_{\text{in}} = \int_{t_0}^{t_0+t'} \int_{L/4-\lambda/10}^{L/4+\lambda/10} \left| B_y^2 + B_z^2 \right| \mathrm{d}x \, \mathrm{d}t, \tag{8}$$

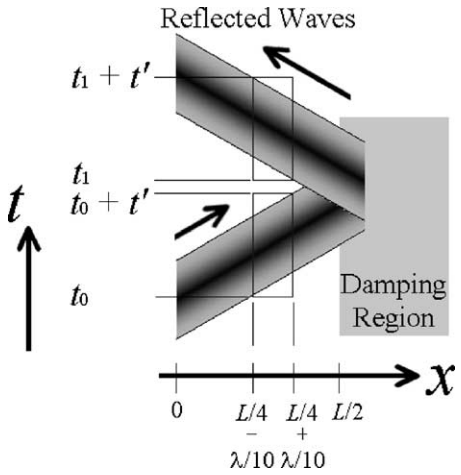

Fig. 6. We specify two regions in the space-time plane covering the same size of passage of incident and reflected waves, respectively. We define intensity of incident and reflected waves by integration of magnetic field energy in the specified regions. L and λ represent length of the physical region and wave length of light mode, respectively, t_0 and t_1 represent times when incident and reflected waves come into each picked up region, respectively.

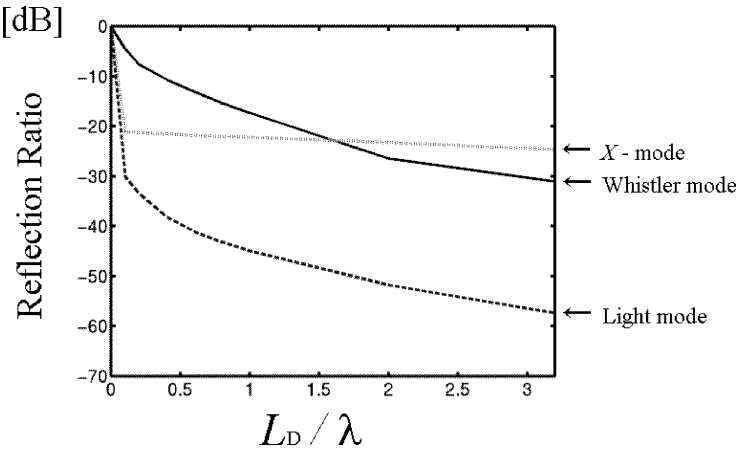

Fig. 7. Reflection ratio as functions of length of the damping region L_D for light mode, whistler mode and X-mode waves, respectively. $\lambda = 314$ grid represents wave length of light mode. For whistler mode, $\Pi_e/\Omega_e = 1.0$. For X-mode, $\Pi_e/\Omega_e = 0.25$.

$$I_{\text{reflect}} = \int_{t_1}^{t_1+t'} \int_{L/4-\lambda/10}^{L/4+\lambda/10} \left| B_y^2 + B_z^2 \right| \mathrm{d}x\, \mathrm{d}t, \tag{9}$$

$$t' = \frac{\lambda}{5v_g} + \frac{2\pi}{\omega_J}, \tag{10}$$

where v_g is group velocity of the waves. We show the reflection ratio of three plasma waves for different length of the damping regions in Fig. 7. The dashed, solid and dotted line correspond to light mode, whistler mode and X-mode waves, respectively. The length of the damping regions is normalized by the wavelength of light mode λ.

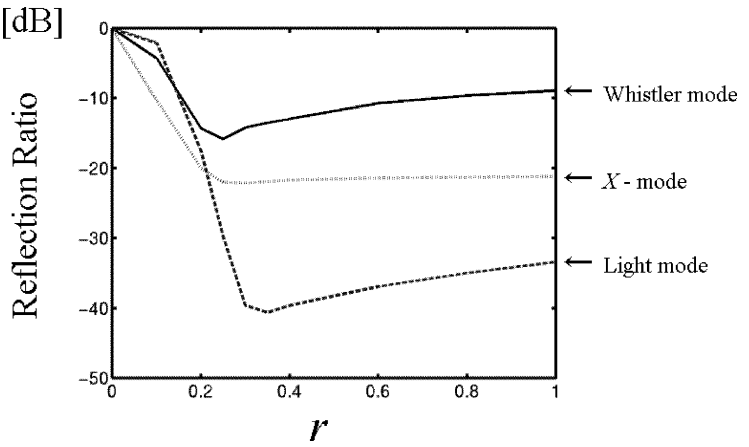

Fig. 8. Reflection ratio as functions of r in (5) for light mode, whistler mode and X-mode waves, respectively. $L_{\mathrm{D}} = 64$. Smaller r corresponds to the smaller masking factor.

The conventional masking method gives better absorption for both waves with larger damping regions, as described in Section 1.

As shown in Fig. 5, outgoing waves penetrate only 30% of the damping regions and are reflected near the boundary between the physical region and the damping region. This implies that large part (about 70%) of the damping region is not used for absorption of the waves. When we use a large damping region, gradient masking function becomes small. Therefore, the gradient of masking function is rather important than the size of damping regions. Since change of function value indicates change of a medium where the waves are propagating, a better masking function should be realized with a smaller gradient.

Next, we varying the masking parameter r and change the gradient of the masking function (5), i.e. length of the effective damping regions. Reflection ratio of three plasma waves for different masking factors are shown in Fig. 8. We obtain minimum reflection ratio for light mode, whistler mode and X-mode with $r \simeq 0.35$, 0.25 and 0.3, respectively. As described above, when we use large masking factor, electromagnetic waves are reflected near the boundary between the physical region and the damping region and we cannot have good absorption. By varying r from 1.0 to smaller value, electromagnetic waves can penetrate the damping regions deeply and reflection ratio becomes smaller. When we use too small masking factor, reflection ratio becomes larger because electromagnetic waves can reach the boundary of the system with a finite amplitude and are reflected back into the system.

Let us consider a finite amplitude wave with the following form is propagating in damping regions.

$$B_W(t) = B_{W_0} \exp(-\mathrm{i}\omega_0 t). \tag{11}$$

From the computation (4), time variation of waves amplitude is expressed as

$$\frac{\partial B_W}{\partial t} = \frac{\alpha B_W^{t+\Delta t/2} - B_W^{t-\Delta t/2}}{\Delta t} = (\omega_i - \mathrm{i}\omega_r) B_W, \tag{12}$$

where α is the masking factor (equivalent to f_{M}). From (11) and (12), we obtain the damping ratio ω_i as follows:

$$\frac{\partial B_W}{\partial t} = \frac{\alpha B_W^{t+\Delta t/2} - B_W^{t-\Delta t/2}}{\Delta t} \tag{13}$$

$$= \frac{\alpha \exp(-\mathrm{i}\frac{\omega_0 \Delta t}{2}) - \exp(\mathrm{i}\frac{\omega_0 \Delta t}{2})}{\Delta t} B_{W_0}(-\mathrm{i}\omega_0 t) \tag{14}$$

$$- \left\{ \frac{1-\alpha}{\Delta t} \cos\frac{\omega_0 \Delta t}{2} - \mathrm{i}\frac{1+\alpha}{\Delta t} \sin\frac{\omega_0 \Delta t}{2} \right\} B_{W_0} \exp(-\mathrm{i}\omega_0 t), \tag{15}$$

$$\omega_i = \frac{1-\alpha}{\Delta t}\cos\frac{\omega_0\Delta t}{2}. \tag{16}$$

By assuming Δt is small enough, the damping ratio normalized by the driving frequency ω_0 is given by

$$\frac{\omega_i}{\omega_0} = \frac{1-\alpha}{\omega_0\Delta t}. \tag{17}$$

Since the amplitude variation propagates at a group velocity, the spatial damping ratio k_i ($k = k_r + \mathrm{i}k_i$) is given by

$$k_i = \frac{\omega_i}{v_g} = \frac{1-\alpha}{v_g\Delta t}. \tag{18}$$

We define an 'effective' spatial damping ratio in damping regions as

$$\int_0^{L_\mathrm{D}} k_i\,\mathrm{d}x = L_\mathrm{D}\int_0^1 \frac{r^2x^2}{v_g\Delta t}\,\mathrm{d}x = \frac{N_\mathrm{D}r^2}{3v_g\frac{\Delta t}{\Delta x}}, \tag{19}$$

where we replace α by $1-r^2x^2$. $v_g\frac{\Delta t}{\Delta x}$ represents a group velocity of waves in the simulation. We call $v_g\frac{\Delta t}{\Delta x}$ an effective group velocity. We have performed simulations with various combination of size of damping region N_D, the masking parameter r and the effective velocity $v_g\frac{\Delta t}{\Delta x}$. We found that the best masking parameter r_0 satisfies the following relation

$$\frac{N_\mathrm{D}r_0^2}{3v_g\frac{\Delta t}{\Delta x}} \simeq 3.3. \tag{20}$$

Effect of the masking method (reflection ratio) also depends on other values besides the effective group velocity, such as number of grid points for a damping region N_D, effective frequency $\omega\Delta t$ and effective wave number $k\Delta x$. From Eqs. (17) and (18), we need larger damping regions to absorb those waves whose frequency is smaller or whose group velocity is slower.

3. Phase retardation

In this section, we introduce another masking factor in Eqs. (4). We can separate the right-hand side of the time difference form of Maxwell's equations into two parts. The first part represents original field values, i.e. electromagnetic fields at the previous time step (at time $t-\frac{\Delta t}{2}$). The second (at time t) represents the increments of the electromagnetic fields for one time step. We use two masking parameters r_d and r_r, and apply the masking function (5) with the different masking parameters as shown in the following form:

$$\left.\begin{aligned}
\boldsymbol{B}^{t+\Delta t/2}(x) &= f_\mathrm{M}(x,r_d)\cdot\left(\boldsymbol{B}^{t-\Delta t/2}(x) - \Delta t\left(\nabla\times\boldsymbol{E}^t(x)\right)\cdot f_\mathrm{M}(x,r_r)\right)\\
\boldsymbol{E}^{t+\Delta t/2}(x) &= f_\mathrm{M}(x,r_d)\cdot\left(\boldsymbol{E}^{t-\Delta t/2}(x) - \Delta t\left(\boldsymbol{J}^t(x) - c^2\nabla\times\boldsymbol{B}^t(x)\right)\cdot f_\mathrm{M}(x,r_r)\right)
\end{aligned}\right\} \tag{21}$$

If $r_r = 0$, i.e. $f_\mathrm{M}(x,r_r) = 1.0$, the above procedure is reduced to the method in Section 2. We analyze effect of each masking factor. We replace both masking functions $f_\mathrm{M}(x,r_d)$ and $f_\mathrm{M}(x,r_r)$ by factors α and β, as follows:

$$\left.\begin{aligned}
\boldsymbol{B}_0^{t+\Delta t/2} &= \boldsymbol{B}^{t-\Delta t/2} - \beta\Delta t(\nabla\times\boldsymbol{E}^t)\\
\boldsymbol{E}_0^{t+\Delta t/2} &= \boldsymbol{E}^{t-\Delta t/2} - \beta\Delta t(\boldsymbol{J}^t - c^2\nabla\times\boldsymbol{B}^t)
\end{aligned}\right\} \tag{22}$$

$$\left.\begin{aligned}
\boldsymbol{B}^{t+\Delta t/2} &= \alpha\boldsymbol{B}_0^{t+\Delta t/2}\\
\boldsymbol{E}^{t+\Delta t/2} &= \alpha\boldsymbol{E}_0^{t+\Delta t/2}
\end{aligned}\right\} \tag{23}$$

Eqs. (23) show that the amplitude (energy) of outgoing waves are gradually reduced in the damping regions at each time step. The masking factor α can be regarded as a 'damping factor'. On the other hand, we cannot absorb outgoing waves when we apply β assuming $\alpha = 1$. In this case, we can obtain the wave equation (24) for light modes, as follows:

$$\left.\begin{aligned} \frac{\partial^2 \boldsymbol{E}}{\partial t^2} &= (\beta \cdot c)^2 \nabla^2 \boldsymbol{E} \\ \frac{\partial^2 \boldsymbol{B}}{\partial t^2} &= (\beta \cdot c)^2 \nabla^2 \boldsymbol{B} \end{aligned}\right\} \quad (0 < \beta < 1). \tag{24}$$

Eqs. (24) shows that electromagnetic waves propagate slower than the light speed with group velocity $v_g = \beta \cdot c$ in damping regions. We also apply the masking factor of β to the current density $\boldsymbol{J}$ to mask motion of plasma particles in the damping regions. All particles are treated as if they are moving with velocities $\beta \cdot v$. In damping regions, therefore, not only waves but also plasmas are moving slower than they move in a physical region. The masking factor of β can be regarded as a 'retarding factor'.

In the new scheme, we can apply various combination of masking factors for both damping and retarding parts varying r_d and r_r. The length of the effective damping region is $1/r_d$ times longer than that of a real damping region. A smaller damping factor corresponds to a longer effective damping region. As we show in Fig. 8, however, when we apply the masking function with too small r, reflection of outgoing waves becomes larger because outgoing waves reach the boundary of the real damping region. By using larger retarding factor, electromagnetic waves propagate more slowly in the damping regions. We expect that reflection of outgoing waves becomes small when we use a combination of smaller r_d and larger r_r.

We present simulation runs based on the new scheme. We apply a combination of a small damping factor and a large retarding factor, $r_d = 0.2$, $r_r = 1.0$, for different length of damping regions. As a simulation result, we show contour maps of magnetic field energy in the $x - t$ space for $L_{\mathrm{D}} = 64$ in Fig. 9. By the new scheme, we obtain almost the same absorption as we obtained by the conventional scheme with 5 times longer damping regions (Fig. 5, $L_{\mathrm{D}}/\lambda = 1.0$). We show reflection ratio of the three plasma waves as functions of length of the damping regions in Fig. 10. The dashed, solid and dotted line correspond to light mode, whistler mode and X-mode waves, respectively. We obtain about -20 dB smaller reflection for light mode and whistler mode waves than those of the conventional method with the same length of the damping regions.

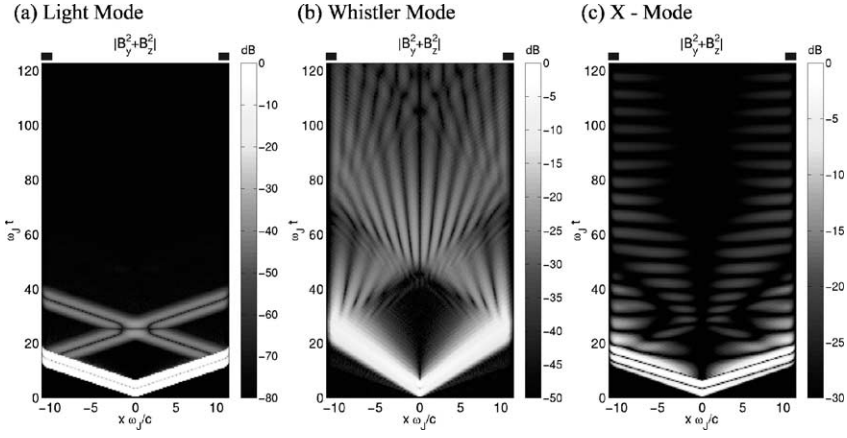

Fig. 9. Spatial and time profiles of magnetic field energy, $|B^2|$, of light mode (left), whistler mode (center), X-mode waves (right), respectively. We apply the improved masking scheme with $r_d = 0.2$, $r_r = 1.0$ to 64 grid points in each damping region. The sizes of the damping region are shown by the lines above the figures.

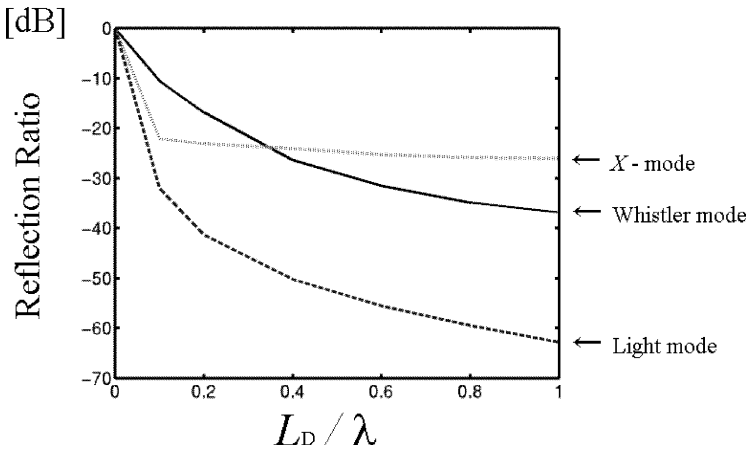

Fig. 10. Reflection ratio as functions of length of the damping region L_D for light mode, whistler mode and X-mode waves, respectively. $\lambda = 314$ represents wave length of light mode.

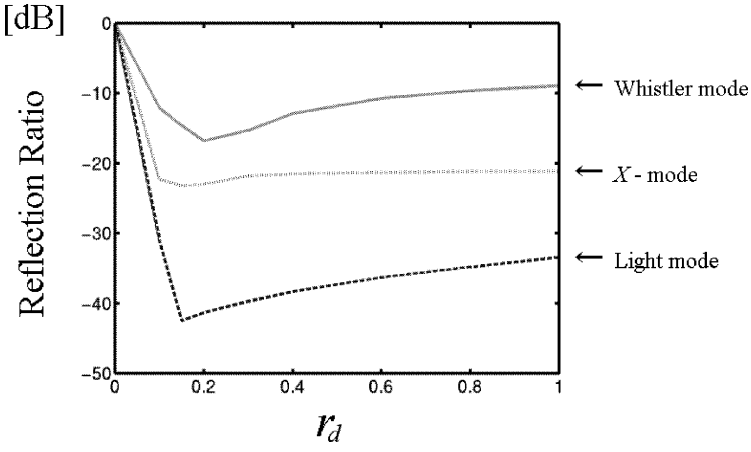

Fig. 11. Reflection ratio as functions of r_d for light mode, whistler mode and X-mode waves, respectively. $L_D = 64$. $r_r = 1.0$. Larger r_d corresponds to larger damping factor.

Next, we investigate the most effective combination of r_d and r_r. Firstly, we vary r_d with $r_r = 1.0$ and $L_D = 64$. The reflection ratio for different r_d is shown in Fig. 11. The best absorption for both three modes are realized with $r_d = 0.15 \sim 0.2$, i.e. the combination of smaller damping factor and larger (largest) retarding factor. As discussed in Section 2, the damping factor that gives the best absorption depends on the numerical group velocity of outgoing waves. Secondly, we vary r_r with $r_d = 0.2$ and $L_D = 64$. The reflection ratio for different r_r is shown in Fig. 12. In this case, the best absorption for both three modes are realized with $r_r \simeq 0.9$. To see effect of retarding factor in detail, we show reflection ratio of light mode as functions of r_r for $r_d = 0.16$, $r_d = 0.2$ and $r_d = 0.4$, respectively, in Fig. 13. For $r_d = 0.4$, we have worse absorption with larger retarding factor. As mentioned in Section 2, when we use larger damping factor ($r_d > r_0 = 0.35$), electromagnetic waves do not reach boundaries of damping regions. By using smaller retarding factor, outgoing waves propagate faster and penetrate damping regions more deeply. For $r_d = 0.16$ and 0.2, on the other hand, the retarding effect is important to absorb outgoing waves. Using larger retarding factor, we have better absorption of outgoing waves. However, too large

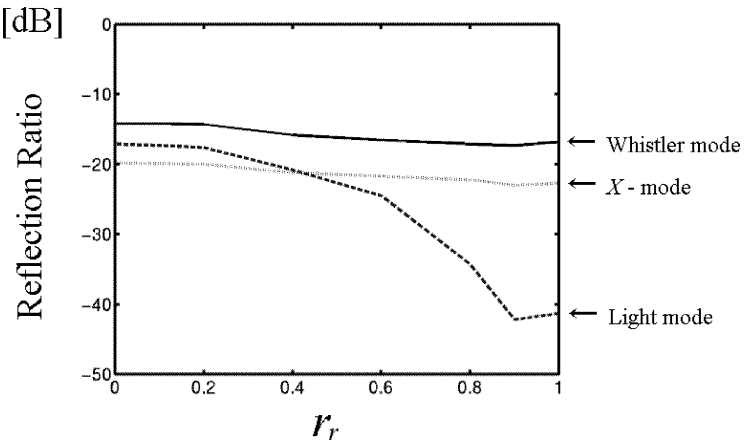

Fig. 12. Reflection ratio as functions of r_r for light mode, whistler mode and X-mode waves, respectively. $L_D = 64$ grid, $r_d = 0.2$. Larger r_r corresponds to larger retarding factor.

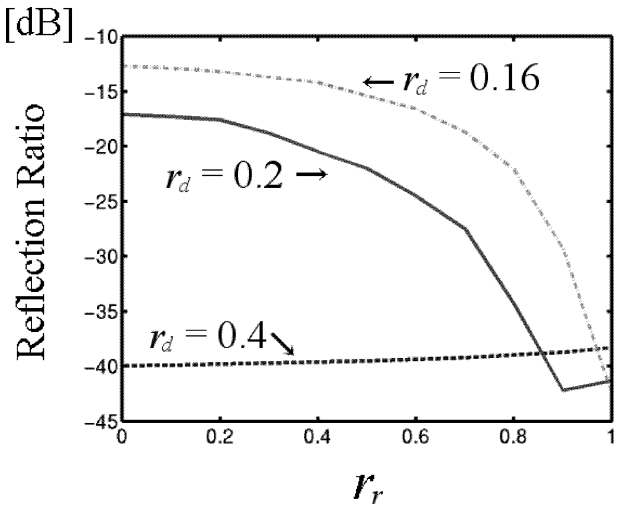

Fig. 13. Reflection ratio as functions of r_r for light mode waves with $r_d = 0.16$, $r_d = 0.2$ and $r_d = 0.4$, respectively.

retarding factor gives reflection rather than absorption for $r_d = 0.2$. For the case with a smaller damping factor ($r_d < 0.35$), electromagnetic waves reach the boundaries of the damping regions before they are absorbed. By using a larger retarding factor, outgoing waves stay longer in damping regions resulting more effective absorption. As we described above, we can have better absorption with the smaller damping factor ($r_d = 0.16$, $r_r = 1.0$: -42.5 dB) than with the larger damping factor ($r_d = 0.4$, $r_r = 0.0$: -40.0 dB), because of longer effective damping regions.

In most cases, the best retarding parameter is $r_r = 1.0$. Because of the retarding effect, however, wave length of outgoing waves gradually becomes shorter ($\lambda = 2\pi c/\omega$) and wave number of the waves becomes larger. When the effective wave number becomes larger than the maximum wave number of the system ($\omega \Delta x/\beta c > k_{\max} = \pi$),

Table 2
Spatial damping ratio $\int_0^{L_D} k_i \, dx$ and reflection ratio Γ for parameters r_d, r_r, N_D and $(c\frac{\Delta t}{\Delta x})$. $\omega_J \Delta t = 0.015$

r_d	r_r	N_D	$c\frac{\Delta t}{\Delta x}$	$\int_0^{L_D} k_i \, dx$	Γ
0.16	1.0	64	0.75	3.09	−42.5 dB
0.15	1.0	64	0.60	3.40	−43.0 dB
0.14	1.0	64	0.45	3.95	−43.2 dB
0.11	1.0	128	0.75	3.64	−54.0 dB
0.1	1.0	128	0.60	3.76	−54.7 dB
0.09	1.0	128	0.45	4.07	−55.3 dB
0.09	1.0	192	0.75	4.08	−61.8 dB

the waves cannot exist in damping regions and are reflected. We can summarize that the best retarding factor (the largest r_r) is given by

$$r_r = \begin{cases} \left(1 - \frac{\omega \Delta x}{c\pi}\right)^{1/2} \frac{N_D}{N_D - 1} & \text{for } \Delta x \geqslant \frac{c\pi}{\omega}\left(1 - \left(\frac{N_D - 1}{N_D}\right)^2\right), \\ 1.0 & \text{for } \Delta x < \frac{c\pi}{\omega}\left(1 - \left(\frac{N_D - 1}{N_D}\right)^2\right). \end{cases} \tag{25}$$

It is noted that the retarding parameter must be $r_r \leqslant 1.0$ because electromagnetic waves cannot propagate faster than the light speed. Using the same idea in Section 2, we compute effective spatial damping ratio of the new scheme, as follows:

$$\begin{aligned} \int_0^{L_D} k_i \, dx &= \int_0^{L_D} \frac{1 - \alpha}{\beta c \Delta t} \, dx = \frac{L_D}{c \Delta t} \int_0^1 \frac{r_d^2 x^2}{(1 - r_r^2 x^2)} \, dx \\ &\simeq \frac{N_D}{c\frac{\Delta t}{\Delta x}} \left(\frac{r_d}{r_r}\right)^2 \left[\frac{1}{2 r_r} \log\left|\frac{1 + r_r x}{1 - r_r x}\right| - x\right]_0^{N_D/(N_D - 1)}, \end{aligned} \tag{26}$$

where we replace α and β by $1 - r_d^2 x^2$ and $1 - r_r^2 x^2$, respectively. We investigate the best combination of r_d and r_r, and compute spatial damping ratio $\int_0^{L_D} k_i \, dx$. We list $\int_0^{L_D} k_i \, dx$ and reflection ratio Γ for typical parameters r_d, r_r, N_D and $(c\frac{\Delta t}{\Delta x})$ with an effective frequency $\omega_J \Delta t = 0.015$ in Table 2. As indicated in Table 2, by setting that $\int_0^{L_D} k_i \, dx = 3.0 \sim 4.0$, the best r_d for light mode can be obtained.

4. Summary and conclusion

The conventional masking method can suppress reflection of various plasma waves at boundaries. The conventional method requires substantial damping regions to absorb outgoing waves. Larger damping regions are realized by using larger computer memory. We first introduced a new masking parameter to change the effective length of damping regions. Characteristics of the method with the effective damping regions are summarized as follows:

- Assigning size of a damping region N_D and effective group velocity $v_g \frac{\Delta t}{\Delta x}$, we can obtain the best masking parameter r_0 from Eq. (20), namely,

$$r_0 \simeq \sqrt{10 \frac{v_g \frac{\Delta t}{\Delta x}}{N_D}}. \tag{27}$$

- Effect of the masking method depends on the following values: frequency, group velocity of waves and size of damping regions. We need large damping regions to absorb the waves with smaller numerical frequency or with slower numerical group velocity.

We separate the time difference form of Maxwell's equations in two parts. The first part represents the original electromagnetic field values. The second part represents the increments of electromagnetic fields. We introduce another masking factor into the increments and apply two masking factors as shown in Eqs. (21). The characteristics of the improved masking method are summarized as follows:

- Masking the new electromagnetic field values given by sum of the original field values and increments, we can absorb the energy of outgoing waves in damping regions. The masking factor for the new field values is regarded as a damping factor.
- By masking the increments of electromagnetic fields, electromagnetic waves propagate slowly in the damping regions. The masking factor for the increments is regarded as a retarding factor.
- The best absorption of outgoing waves is realized with a combination of a smaller damping factor ($r_d < r_0$) and the largest retarding factor ($r_r \cong 1.0$).

To use the new masking method,

1. Apply the damping and retarding factors to the Maxwell's equations as shown in Eqs. (21).
2. Specify the size of damping regions N_{D}. The better absorption is given by using longer damping regions.
3. Determine the retarding parameter r_r from Eq. (25).
4. Determine the damping parameter r_d. By setting that Eq. (26) is equal to 3.0∼4.0, the best r_d can be obtained.

The new scheme gives better absorption than the conventional scheme with the same length of damping regions. Even when we use the new scheme with one-fifth of the damping regions used in the conventional scheme, we can obtain almost the same absorption. It is possible to make simulation code faster by reducing the size of damping regions.

As we mentioned above, efficiency of the masking method depends on frequency, group velocity of waves and size of damping regions. Characteristics on such values should be investigated in future. In the present study, we performed simulations for only the three modes. In plasmas, there exist many electromagnetic waves which have various phase velocities and polarizations. Optimization of the masking method for electrostatic waves or low-frequency waves such as ion modes is left as a future study. In most cases, however, light mode waves are always present in electromagnetic particle simulations. The group velocity of light modes is the fastest, implying that the absorbing boundary condition is the most stringent for the light modes. Thus the characteristics of reflection of the light modes with the new masking method listed in Table 2 are useful in most of electromagnetic particle simulations.

It is noted that there is a similar absorbing boundary method proposed by Berenger and well known as the Perfectly Matched Layer (PML) method [7]. In the PML method, the light modes are absorbed in a resistive layer attached at boundaries. Electric and magnetic conductivity in this layer are determined so that impedance is perfectly matched with that in vacuum. In plasmas, such impedance matching conditions are not satisfied because of the fluctuating conduction current density formed by the thermal charged particles. Thus the complete PML is not realized in the electromagnetic particle simulations. We also note that there is no phase retardation in the PML method, and that the light modes propagate with the light speed in the matched layer. However, it is obvious from our results that the phase retardation affects the efficiency of plasma wave absorption. Incorporation of the phase retardation effect in the PML method may yield better absorption of plasma waves, which is also left as a future study.

Acknowledgements

We thank T. Tominaga for useful documents on the conventional masking method. We also thank H. Usui for useful discussions. The computer simulations were performed on the KDK computer system at Radio Science Center for Space and Atmosphere, Kyoto University.

References

[1] H. Matsumoto, T. Sato, Computer Simulation of Space Plasmas, Terra Sci., Tokyo, 1984.
[2] C.K. Birsall, A.B. Langdon, Plasma Physics via Computer Simulation, McGraw-Hill, New York, 1985.
[3] E.L. Lindman, J. Comput. Phys. 18 (1975) 66.
[4] I. Orlanski, J. Comput. Phys. 21 (1976) 251.
[5] T. Tajima, V.C. Lee, J. Comput. Phys. 42 (1981) 406.
[6] Y. Omura, H. Matsumoto, in: H. Matsumoto, Y. Omura (Eds.), Computer Space Plasma Physics, Terra Sci., Tokyo, 1993, p. 21.
[7] J.P. Berenger, J. Comput. Phys. 114 (1994) 185.